AGU PUBLICATIONS

Geophysical Research Letters

RESEARCH LETTER
10.1002/2017GL073702

Key Points:
- We apply the latest experimental result of ilmenite to the lunar mantle dynamics
- The weak ilmenite rheology leads to a viscosity reduction of ilmenite-bearing cumulates
- A 1 order magnitude of viscosity reduction in the cumulate mantle causes the upwelling dynamics to a dramatic change

Supporting Information:
- Supporting Information S1

Correspondence to:
N. Zhang,
nan_zhang@pku.edu.cn

Citation:
Zhang, N., N. Dygert, Y. Liang, and E. M. Parmentier (2017), The effect of ilmenite viscosity on the dynamics and evolution of an overturned lunar cumulate mantle, *Geophys. Res. Lett.*, *44*, 6543–6552, doi:10.1002/2017GL073702.

Received 3 APR 2017
Accepted 10 JUN 2017
Accepted article online 14 JUN 2017
Published online 3 JUL 2017

The effect of ilmenite viscosity on the dynamics and evolution of an overturned lunar cumulate mantle

Nan Zhang[1,2,3], Nick Dygert[1,4,5], Yan Liang[1], and E. M. Parmentier[1]

[1]Department of Earth, Environmental and Planetary Sciences, Brown University, Providence, Rhode Island, USA, [2]Key Laboratory of Orogenic Belts and Crustal Evolution, Institution of Earth and Space Sciences, Peking University, Beijing, China, [3]Department of Applied Geology, Curtin University, Perth, Western Australian, Australia, [4]Jackson School of Geosciences, University of Texas at Austin, Austin, Texas, USA, [5]Department of Earth and Planetary Sciences, University of Tennessee, Knoxville, Knoxville, Tennessee, USA

Abstract Lunar cumulate mantle overturn and the subsequent upwelling of overturned mantle cumulates provide a potential framework for understanding the first-order thermochemical evolution of the Moon. Upwelling of ilmenite-bearing cumulates (IBCs) after the overturn has a dominant influence on the dynamics and long-term thermal evolution of the lunar mantle. An important parameter determining the stability and convective behavior of the IBC is its viscosity, which was recently constrained through rock deformation experiments. To examine the effect of IBC viscosity on the upwelling of overturned lunar cumulate mantle, here we conduct three-dimensional mantle convection models with an evolving core superposed by an IBC-rich layer, which resulted from mantle overturn after magma ocean solidification. Our modeling shows that a reduction of mantle viscosity by 1 order of magnitude, due to the presence of ilmenite, can dramatically change convective planform and long-term lunar mantle evolution. Our model results suggest a relatively stable partially molten IBC layer that has surrounded the lunar core to the present day.

Plain Language Summary The Moon's mantle is locally ilmenite rich. Previous models exploring the convective evolution of the lunar mantle did not consider the effects of ilmenite viscosity. Recent rock deformation experiments demonstrate that Fe-Ti oxide (ilmenite) is a low viscosity phase compared to olivine and other silicate minerals. Our modeling shows that ilmenite changes the lunar mantle plume process. An ilmenite-rich layer around the lunar core would be highly stable throughout geologic time, consistent with a partially molten, low viscosity layer around the core inferred from seismic attenuation and tidal dissipation.

1. Introduction

Lunar cumulate mantle overturn and subsequent upwelling of overturned mantle cumulates have been proposed to explain the thermochemical evolution of the Moon after lunar magma ocean solidification [*Hess and Parmentier*, 1995; *Papike et al.*, 1998; *Zhong et al.*, 2000]. These models address the origin of fundamental features such as the location of present-day nearside seismicity, cessation of lunar dynamo, and the contraction history of the Moon [e.g., *Binder*, 1982; *Nyquist and Shih*, 1992; *Lucey et al.*, 1998; *Nakamura*, 2003; *Stegman et al.*, 2003; *Lawrence et al.*, 2008]. Attempts to explain the asymmetrical distribution of lunar mare basalts on the nearside of the Moon, which is the most prominent lunar surface feature, have focused on upwelling of overturned lunar magma ocean cumulates [*Zhong et al.*, 2000; *Zhang et al.*, 2013a, 2013b].

The present study addresses how such upwellings of previously overturned mantle cumulates may influence lunar evolution. In particular, we evaluate the implications of recent ilmenite deformation experiments on the viscosity of the ilmenite-bearing cumulates (IBCs) [*Dygert et al.*, 2016] for upwelling of an overturned cumulate mantle.

The origin of the IBC lithology comes from our understanding of lunar magma ocean solidification [e.g., *Hess and Parmentier*, 1995; *Elkins-Tanton et al.*, 2011]. After the giant impact [e.g., *Warren*, 1985; *Canup*, 2012; *Ćuk and Stewart*, 2012], the lunar magma ocean crystallized mafic minerals, then plagioclase, and upon reaching 95% solidification, became saturated in ilmenite, along with Fe-rich clinopyroxene [*Ringwood and Kesson*, 1976; *Snyder et al.*, 1992; *Lin et al.*, 2017]. Under the buoyant plagioclase crust, the dense cumulates (ilmenite

and clinopyroxene) continued to crystallize, concentrating incompatible elements including K, REE, P, U, and Th (commonly referred to as KREEP). Because ilmenite and Fe-rich clinopyroxene are dense, the resultant mineral stratification would have been gravitationally unstable. By solid-state convection, the dense late magma ocean cumulates may have sank into the lunar interior in a process termed cumulate mantle overturn. Some fraction of KREEP, including the heat producing elements (HPE) K, U, and Th, would have been entrained during overturn and carried into the lunar interior along with the IBC. Under specific conditions, intrinsically dense, HPE-rich overturned IBC may have heated up sufficiently to allow thermal buoyancy to generate upwelling plumes [*Zhang et al.*, 2013a; *Stegman et al.*, 2003; *Zhong et al.*, 2000].

The relative viscosities of the overturned IBC and overlying harzburgite mantle play a fundamental role in determining the convective planform and the wavelength of IBC upwelling [e.g., *Zhong et al.*, 2000; *Zhang et al.*, 2013a, 2013b]. In two recent studies, *Zhang et al.* [2013a, 2013b] explored the effects of various temperature-dependent viscosities on the mantle-core dynamics after the overturn. They noticed that an IBC-rich layer, with a moderately smaller viscosity than the harzburgite mantle, is most likely to form a single large upwelling plume. In contrast, a much less viscous IBC-rich layer experiences vigorous internal convection, largely remaining at the core-mantle boundary to the present day. According to *Zhang et al.* [2013a], in a scenario where IBC viscosity is moderately sensitive to temperature (effective activation energy = 100 kJ/mol), high IBC temperatures induce a viscosity ~100 times lower than the overlying mantle, which produces a large-scale single plume. In scenarios where the IBC viscosity is highly sensitive to the temperature (effective activation energy $\geq$200 kJ/mol), lower viscosity IBC layers (by more than 3 orders of magnitude lower than the overlying harzburgite) is cooled by vigorous internal convection, efficiently dissipating heat into the overlying mantle; thus, they have little thermal buoyancy. In this scenario, the IBC largely remain at the core-mantle boundary to the present day [*Zhang et al.*, 2013a].

A recent experimental study places constraints on the viscosity of the IBC-like lithologies for the first time. In a Griggs rock deformation apparatus, *Dygert et al.* [2016] deformed pure synthetic ilmenite in dislocation creep and used the experimental observations to parameterize a dislocation creep flow law for ilmenite. At mantle temperatures and differential stresses, the flow law predicts that ilmenite is more than 3 orders of magnitude weaker than dry olivine. To investigate the effect of ilmenite on the viscosity of the IBC (which probably contain 3–9 wt % ilmenite), *Dygert et al.* [2016] calculated viscosities for ilmenite-olivine aggregates using several mixing models (Figure 1a). These models illustrate the large uncertainty in the viscosity of ilmenite-olivine aggregates (and by extension, the IBC). However, experimental studies that measured the rheology of multiphase aggregates composed of other phases [*Jordan*, 1987; *Tokle, et al.*, 2016] have shown that aggregates approach the lower (isostress or Reuss) bound [*Reuss*, 1929] after extents of deformation relevant to lunar mantle convection, even with small proportions of a low-viscosity phase. Experiments on ilmenite-olivine aggregates are in progress to better evaluate whether the ilmenite-olivine system behaves similarly. Current experimental work suggests that a lower bound on IBC viscosity may be assumed using the isostress mixing model (green square, Figure 1a). Making a more conservative assumption, here we apply the viscosity shown by the blue square in Figure 1a as the IBC viscosity to study the dynamic stability of overturned mantle cumulates. Our model formulation differs from *Zhang et al.* [2013a, 2013b] in that we incorporate a composition-dependent viscosity correction to take into account the weak ilmenite effect. With the model calculation, we examine fate of a weak, IBC-rich layer surrounding the lunar core.

2. Model Formulation

The thermochemical evolution of overturned mantle cumulates is investigated in a numerical model of three-dimensional spherical geometry. Except for the additional consideration of the IBC viscosity, our models are the same as that described in *Zhang et al.* [2013a, 2013b]. Our model incorporates the evolution of both mantle and core. The mantle part has an IBC-rich layer with lower viscosity and higher density on the core-mantle boundary (CMB). The mantle thermal Rayleigh number is given to 1.3×10^6 [*Zhang et al.*, 2013a]. This mantle with spherical shell geometry couples the underlying spherical core through thermal interaction. The core is treated as a parameterized solidifying Fe-FeS alloy. Our models use $12 \times 64 \times 48 \times 48$ elements mesh based on CitcomS [*Zhong et al.*, 2008], which gives an azimuthal resolution of 14 km and radial resolution of 22 km. The overturn process determines the ilmenite fraction and density of the IBC-rich layer. A systematic estimation recommends the ilmenite fraction in a range of 3–9 wt %, and

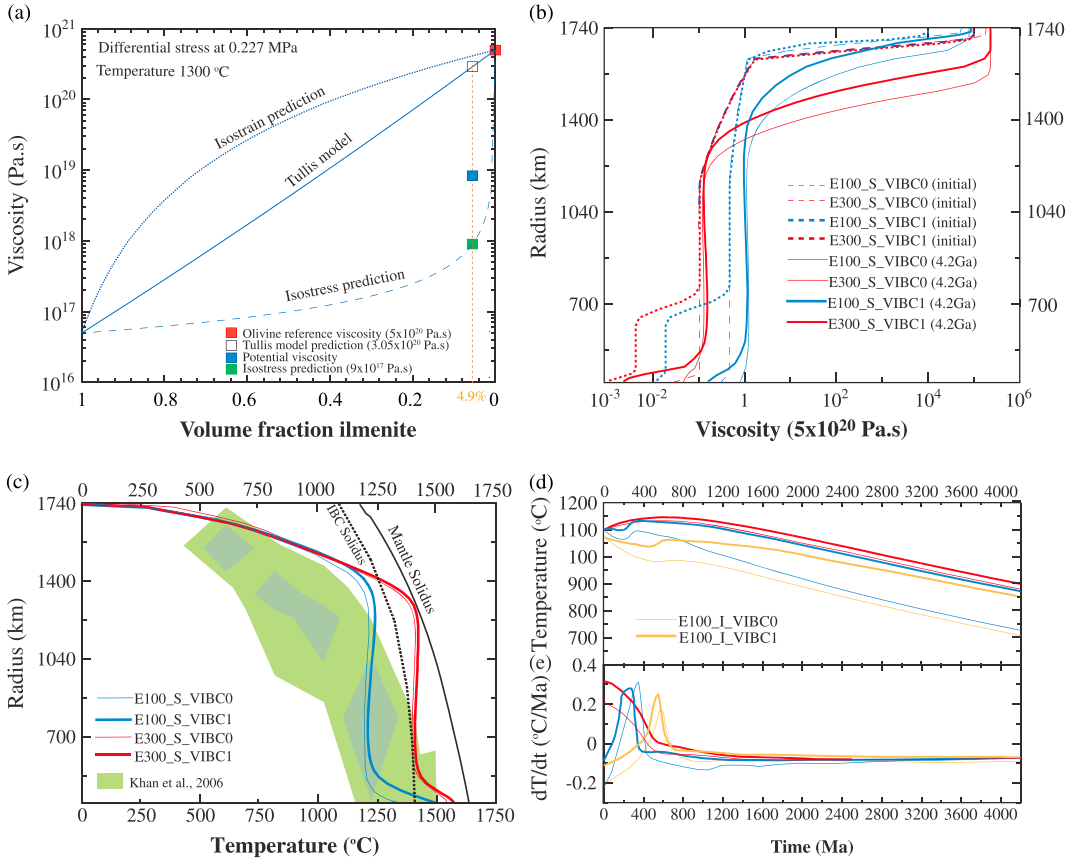

Figure 1. (a) The viscosities of a dry ilmenite-olivine aggregate calculated using end-member flow laws [*Dygert et al.*, 2016; *Hirth and Kohlstedt*, 2003]. The solid line is the aggregate viscosity calculated from the model of *Tullis et al.* [1991]. The dashed and dotted lines are the isostress and isostrain bounds, respectively. If the overturned IBC has 6 wt % (4.9 vol %) ilmenite, its viscosity may be approximated by the blue square in this figure. (b and c) The variations of azimuthally averaged viscosity and temperature as a function of radius. The dashed curves are for the initial state, and the solid curves are for the present day. (c) The IBC solidus is modified from *Yao and Liang* [2012]. (d and e) The evolution of average temperature and cooling rate of the top 520 km mantle for the selected cases.

hence, the IBC density contrast from the harzburgite mantle within the range of 1–4% [e.g., *Hess and Parmentier*, 1995; *Zhang et al.*, 2013a].

The distribution of HPE in the deep mantle is determined by the KREEP abundance in the IBC-rich material [*Hess and Parmentier*, 1995]. The proportion of KREEP-bearing cumulates, flowing with the IBC, is also determined by the overturn process. Our early work explored a series of reasonable KREEP fractions in the IBC-rich material. The bulk U and Th abundances are used to estimate the heat generation rate in KREEP. The bulk U and Th contents at the present-day are taken to 25.7 ppb and 102.8 ppb (Th/U = 4) [e.g., *Taylor*, 1982]. The Moon is highly depleted in the volatile element K [*Wang and Jacobsen*, 2016; *Albarede et al.*, 2014; *Jones and Palme*, 2000]. Our test model shows that K content (based on K/U ratio of 2500 [*Taylor*, 1982]) does not affect the instability of IBC-rich layer (Table S1 in the supporting information). In the models presented in this study, we neglect K contribution to the thermal budget. The decay rates of heat generations are taken from *Turcotte and Schubert* [2002].

The relative abundance of HPE in the dense IBC-rich layer is important in determining the timing at which the IBC-rich material becomes buoyant. Based on our previous calculations [*Zhang et al.*, 2013a], we constrain model parameters to a range that can generate the mare basalts around ~3.9 Ga. Hence, the IBC-rich layer in our reference case has 6 wt % of ilmenite, which leads to 2.6% density contrast to the overlying mantle. The IBC-rich layer also includes 50% of the lunar HPE budget (through KREEP) [*Zhang et al.*, 2013a]. The upper mantle maintains the remaining KREEP and HPE at the base of the crust. The effect of different combinations of HPE and IBC fractions in the IBC-rich material is further discussed in section 4.

Here to demonstrate the potential weakening effect of ilmenite and to compare with our recent study, we consider the following Arrhenius-type flow law for the mixture viscosity

$$\eta(T, C_{\mathrm{IBC}}) = [C_{\mathrm{IBC}}\eta_{\mathrm{IBC}} + (1 - C_{\mathrm{IBC}})\,\eta_{\mathrm{ref}}] \exp\left(\frac{E}{RT} - \frac{E}{RT_{\mathrm{ref}}}\right) \quad (1)$$

where $\eta_{\mathrm{ref}} = 5 \times 10^{20}$ Pa s is the viscosity at the reference temperature (T_{ref}) for IBC-free harzburgite, η_{IBC}=7.5 × 10^{18} Pa s is IBC-rich material viscosity estimated from the experiments of *Dygert et al.* [2016] (Figure 1a), C_{IBC} is the IBC fraction, E is the effective activation energy, and R is the gas constant. The reference temperature is 1300°C [*Zhang et al.*, 2013a]. The viscosity of 7.5 × 10^{18} Pa s is estimated from Figure 1a for a dunite with 6 wt % or 4.9 vol % ilmenite, which serves as a reference viscosity for the ilmenite-bearing harzburgite in this study. The major difference from our previous studies is the inclusion of the IBC-rich material viscosity through the preexponential factor. In the absence of laboratory data on mixture rheology, we use a common linear interpolation between reference viscosities for the IBC-rich and IBC-free harzburgites. More physically realistic treatments of multiphase aggregate viscosity would incorporate texture-dependent strain partitioning considerations and composition-dependent elemental exchange between phases [cf. *Dygert et al.*, 2016]. Experimental data needed to parameterize such models are currently unavailable. Equation (1) should provide a reasonable approximation of the viscosity of IBC-harzburgite mixtures.

If strain in the IBC is predominantly accommodated by the ilmenite component of the mixture, the bulk IBC activation energy may be similar to or a few tens of percent lower than the activation energy of the harzburgite. Experiments are underway to characterize the rheology of ilmenite, which is a long-term process and will ultimately allow us to place better constraints on the viscosity of IBC [*Tokle et al.*, 2017]. As a first attempt, here we assume that the activation energy of the IBC is the same as that for the ilmenite-free harzburgite. A lower effective activation energy is implemented in equation (1) to take into account the influence of power law viscosity [e.g., *Christensen*, 1984], which was examined and discussed in detail in *Zhang et al.* [2013a]. These effective activation energies correspond to non-Newtonian activation energies of ~330–670 kJ/mol [*Karato and Wu*, 1993; *Hirth and Kohlstedt*, 2003]. Thus, our simulations test lower and upper bounds on possible activation energies for the lunar mantle.

Both the temperature- and composition-dependent viscosities have dominant effect on the stability of IBC-rich layer. The dense IBC-rich layer becomes unstable when density decreases due to HPE-induced thermal expansion, which can compensate for its higher compositional density. Heating as well as the presence of ilmenite reduce the viscosity of the IBC-rich material. After the viscosity becomes low, the advection inside the IBC-rich layer efficiently transfers heat into the overlying mantle, limiting IBC temperature rise and suppressing or preventing upwelling of the IBC layer. Thus, sufficiently modest temperature and composition dependences are necessary for the IBC-rich layer to develop a long-wavelength instability as well as upwelling.

The initial thermal state of our model is derived from the peridotite solidus. This solidus is truncated at the top 90 km with a cold thermal boundary layer. We consider two scenarios for the initial temperature distribution: the regular and inverted peridotite solidus [*Zhang et al.*, 2013a]. The latter assumes overturn as an adiabatic process. The resultant temperature profile is inverted from solidus [*Elkins-Tanton et al.*, 2002]. Core solidification is parameterized following that of *Stevenson and Yoder* [1981]. Inner core growth releases latent heat. Our previous study [*Zhang et al.*, 2013a] preferred a core sulfur content of 7 wt %, which could produce an ~240 km radius inner core, consistent with seismic observations [e.g., *Weber et al.*, 2011].

3. Results

In total, six models are presented in this study. They are organized in three groups (Table S1). The initial thermal state of our first and second groups starts from the same convective temperature profile, truncated by the mantle solidus. The third group adopts the inverted mantle solidus as the initial temperature (supporting information). The first and third groups have E = 100 kJ/mol [*Zhang et al.*, 2013a; *Christensen*, 1984]. The second group has E = 300 kJ/mol. Previous simulations that assume a composition independent rheology [*Zhang et al.*, 2013a] found that the IBC layer remains at the lunar CMB (i.e., stable) for the larger effective viscosity but upwells as a single chemical plume for the case of the smaller effective viscosity. For each of these three groups, we add one more case with IBC-dependent viscosity. We label our cases based on the

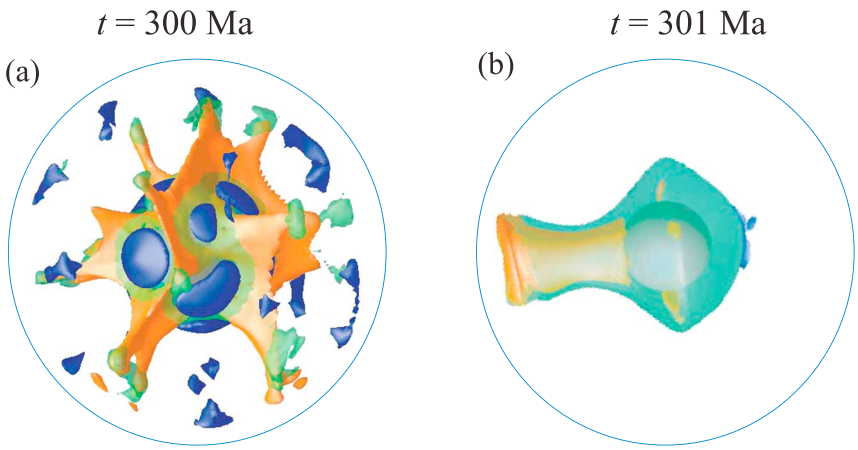

Figure 2. The contrast of 3-D thermochemical structures between cases (a) E100_S_VIBC1 and (b) E100_S_VIBC0 after 301 Ma. The 3-D thermal structures are plotted as isosurfaces of residual temperature with contour levels of −0.07 (blue) and 0.07 (orange). The chemical structure (i.e., IBC) is plotted as isosurfaces of compositional field (green). The surface and core-mantle boundary are plotted as a blue curve and red spherical surface.

effective activation energy, the initial temperature condition, and the viscosity of IBC-rich material. For example, E100_S_VIBC1 refers to a case with E = 100 kJ/mol, peridotite solidus as the initial thermal condition (designated by S), and with IBC-dependent viscosity (1), while E100_I_VIBC0 refers to a case with E = 100 kJ/mol, inverted peridotite solidus as the initial thermal condition (I), and without IBC-dependent viscosity (marked by 0).

The first group of two models examines the effects of the IBC-dependent viscosity on the stability of IBC-rich material in the lowermost mantle. We start from the reference case E100_S_VIBC1, which includes IBC-dependent viscosity. In Figure 1b, the thick dashed blue curve shows the initial viscosity profile. The reduction of viscosity in the layer right above CMB is a manifestation for IBC-dependent viscosity. Randomly perturbing the initial thermal state by a magnitude 1% of total temperature difference, we run the model for 4.2 Ga. Due to its weaker rheology, radiogenic heating within the IBC-rich layer causes a strong internal advection within the layer which prevents the IBC-rich layer from gaining enough thermal buoyancy to rise as a single plume. Therefore, the IBC-rich layer remains largely on CMB, while small-scale thermochemical plumes are generated on its top (Figure 2a). As the model evolves, this layer is slowly mixed with the mantle above. After the IBC-rich layer is entrained and deformed to a thin pile, the thermal field evolves to a structure dominated with degree 1 spherical harmonics. At the end of 4.2 Ga of thermal evolution, an IBC-rich pile, covering 48% CMB area, remains on a hemisphere of CMB (Figure S1b). The CMB temperature decreases to 1450°C (Table S1) at the present day. We quantify the (azimuthally averaged) temperature profiles with time for case E100_S_VIBC1 (Figure 3a). The case shows that the mantle and the IBC-rich layer remain warm all the time because the IBC-rich material in case E100_S_VIBC1 does not advect through the overlying mantle (Figure 3a).

Case E100_S_VIBC0 differs from E100_S_VIBC1 in that the IBC-dependent viscosity is not incorporated. This case reproduces the reference case from our previous study (H50E100V5e20 in *Zhang et al.* [2013a]). The initial viscosity profile of E100_S_VIBC0 is shown in Figure 1b (thin dashed blue curve). During the model evolution, the IBC-rich layer behaves totally different. After ~301 Myr, the IBC-rich material gains enough buoyance, growing to a single plume. Correspondingly, a small cold downwelling is formed in the opposite CMB (Figure 2b). After ~600 Myr, the plume hemisphere has the IBC-rich material scattering everywhere. At the end of 4.2 Ga of thermal evolution, small IBC-rich accumulations stay on CMB, covering 17% of CMB area (supporting information Figure S1a). The CMB temperature cools to 1330°C (Figure 1c, thin solid blue curve). This CMB temperature is much lower than case E100_S_VIBC1 (1450°C) because of the upwelling of unstable IBC-rich material (cf. thick and thin blue curves in Figure 1c). The final viscosity profile corresponds to a major thickening of the lunar lithosphere (Figure 1b, thin solid blue curve). The average temperature profiles of case E100_S_VIBC0 are quantified in the plume hemisphere mantle, and its opposite hemisphere. The plume hemisphere is defined with respect to the plume axis. Figure 3b displays the temperature evolution of the

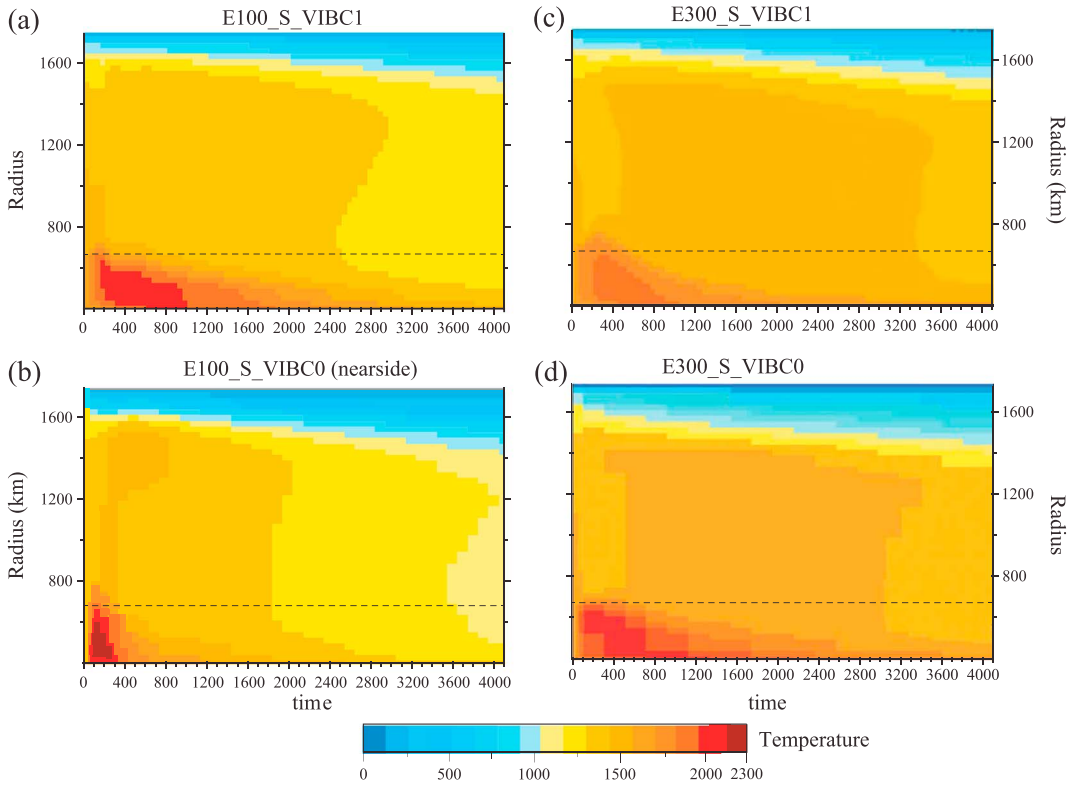

Figure 3. The evolution of azimuthally averaged temperature for four cases from Groups 1 and 2, with initial mantle solidus temperature condition. Temperatures for the cases (a) E100_S_VIBC1, (c) E300_S_VIBC1, and (d) E300_S_VIBC0 are presented with the global average, whereas temperatures for case (b) E100_S_VIBC0 is presented with temperature profile in its plume hemisphere.

plume hemisphere (the temperature evolution of opposite hemisphere is shown in supporting information Figure S2b). Radiogenic heating within the IBC-rich layer results in a rapid temperature rise before 250 Ma. After acquiring enough thermal buoyancy, the IBC-rich layer rises up to form a single upwelling to shallow mantle, resulting in an increase in temperature beneath the thermal boundary layer between 250 and 600 Ma (Figure 3b). The deep red regions in Figures 3a and 3b demonstrate the different evolution of the IBC-rich layers. As discussed in the previous paragraph, the weak IBC rheology in case E100_S_VIBC1 prevents the accumulation of thermal buoyancy in the IBC-rich layer (i.e., less dark red in Figure 3a compared to Figure 3b).

The second group includes two cases. Both have an effective activation energy E = 300 kJ/mol (Table S1). Case E300_S_VIBC1 includes the lower IBC viscosity, while case E300_S_VIBC0 does not. The two cases have very low initial viscosity within the IBC-rich layer, with viscosity for case E300_S_VIBC1 being at least 10 times lower than E300_S_VIBC0 (Figure 1b, two red dashed curves). Both cases end up with stable IBC-rich layers. These long-lived layers trap HPE in the deep mantle, giving rise to high present-day CMB and mantle temperatures (Figure 1c, red curves, and Table S1). The evolution of globally averaged temperatures for cases with and without IBC viscosity is shown in Figures 1d and 1e, respectively. Among these four simulations, the case E300_S_VISC1 has a hot lower mantle surrounding the core for the longest time.

The third group of models explores effect of different initial temperature conditions. We present two cases with the inverted mantle solidus as the initial temperature condition. Case E100_I_VIBC0 does not include a weaker IBC viscosity, and its initial viscosity profile is shown in Figure S3a (thin yellow dashed curve). Similar to the case E100_S_VIBC0, a plume is generated early and fades with time (Figure S2c). In the case incorporating a lower IBC viscosity in the model (E100_I_VISC1) convection in the IBC becomes vigorous, suppressing degree 1 plume generation. We can summarize these results as suggesting that the initial temperature profile has little effect on long-term lunar convective evolution.

The average temperature at the top of the convecting mantle depends on the stability of the IBC layer and the rheology of the cumulate mantle. The presence of a stable IBC-rich layer on CMB, without regard to its origin, slows down the cooling of the shallow mantle. This is illustrated in Figure 1d for evolution of the average temperature at 520 km depth (thin blue and yellow curves versus other four curves). All the cases with E = 100 kJ/mol experience an initial cooling, followed by a brief warming (blue and yellow curves in Figure 1d). The fast initial cooling is caused by the lack of heat transfer from the deep mantle: the smaller activation energy leads to a larger viscosity in mantle (Figure 1b) and less vigorous convection. Thus, heat transfer from the IBC-rich layer upward to the mantle is slower, compared to those in cases with larger activation energy. The thermal evolution of the upper mantle for the two cases with an initially inverted solidus differs because of their colder initial temperatures (yellow curves in Figure 1d) and correspondingly higher viscosities. The shallow mantles in cases E100_S_VIBC0 and E100_I_VIBC0 cool much faster than those in other four cases during the first 2000 Ma (Figure 1e). Afterward, the thermal boundary layers of the six cases have similar cooling rates of ~0.1°C/Ma (Figure 1e). These cases show that once the IBC-rich layer viscosity is small enough, the cooling rates of the top thermal boundary layer do not show much difference. Cases with the inverted solidus initial condition do not show much difference from cases with a noninverted initial mantle solidus (yellow curves versus blue curves) after the effect of lower initial temperature disappears.

4. Discussion

Our model calculations show that the behavior of the IBC-rich layer can be greatly changed when its rheology is weakened by the presence of ilmenite IBC: lower viscosity intensifies the convective vigor of IBC-rich layer, preventing accumulation of thermal buoyancy in this layer. This is consistent with our earlier study [*Zhang et al.*, 2013a], where we showed that for E = 100 kJ/mol and a relatively small lunar core, the high IBC layer temperature induces an ~2 orders of magnitude viscosity reduction relative to the mantle above, resulting a large-scale single plume. The parameter space for a single plume to develop in our models is generally consistent with previous studies based on simpler analysis of Rayleigh-Taylor instability analysis [e.g., *Zhong et al.*, 2000; *Qin and Zhong*, 2014; *Scheinberg et al.*, 2014]. However, in contrast to Rayleigh-Taylor instability analysis, where the viscosity contrast increases as the activation energy increases, degree 1 upwelling of an IBC-enriched layer in our thermochemical models is suppressed because the activation energy controls the density difference through both the viscosity and the convective vigor. The Rayleigh-Taylor instability has only a constant density difference between two layers, whereas in our more complete model the development of thermal buoyancy is suppressed by the very low viscosity within the IBC-rich layer.

When the ilmenite weakening effect on the IBC-rich layer is considered, the viscosity for this layer with E = 100 kJ/mol is reduced to a range close to that for IBC-free rheologies with E = 300 kJ/mol (thick blue dashed curve and thin red dashed curve in Figure 2a). Although this viscosity reduction is compositional instead of thermal, the net effect is the same: a less buoyant, gravitationally more stable IBC-rich layer on CMB for both cases leads to the absence of a global-scale single plume. This explains the similarities in temperature evolution (Figures 3a and 3d), mantle structure, and shallow mantle cooling (Figure 1d) for the two cases. We note an effective activation energy of 100 kJ/mol corresponds to a non-Newtonian activation energy of ~330 kJ/mol, lower than values commonly assumed for deformation of olivine in dislocation creep (which should be a reasonable proxy for ilmenite-free lunar mantle viscosity) [*Hirth and Kohlstedt*, 2003]. Higher effective energies (e.g., 160 kJ/mol, corresponding to non-Newtonian activation energies of ~500 kJ/mol) would further suppress development of a degree 1 upwelling structure.

Results presented in this study depend on the viscosity of IBC-rich materials and abundance of ilmenite in the IBC. Our model uses the median value of 6 wt % from a reasonable range of 3–9 wt % [*Hess and Parmentier*, 1995; *Zhang et al.*, 2013a; *Zhang*, 2014]. We chose a reference viscosity for the IBC intermediate to the isostress bound and the Tullis model (the blue square in Figure 1). If we use the Tullis model at 4.9 vol % ilmenite as our refrence value for the IBC-rich material, the convection patterns is similar to the case E100_S_VIBC0. The single plume mode is supressed only when the viscosity contrast between the ilmenite-bearing and ilmenite-free harzburgite layers is greater than 1 order of magnitude. This underscores the importance of IBC rheology in determining the dynamics and behavior of the IBC-rich material on lunar CMB. Even at low-volume fractions, ilmenite will efficiently reduce the effective viscosity of the IBC when it accommodates more strain than the stronger silicate phases. Experiments exploring the textural evolution of ilmenite-olivine

aggregates demonstrate that at high strains associated with mantle advection, initially isolated ilmenite inclusions are enjoined to form sheet-like networks that may exert a dominant control on the aggregate rheology [*Dygert*, 2015; *Tokle et al.*, 2016]. Based on textural considerations, at some very low ilmenite fraction, ilmenite inclusions must remain isolated and in such cases, ilmenite would have a small effect on the aggregate viscosity. In these scenarios, the IBC will probably be significantly more viscous than the case with 4.9% ilmenite.

The abundance of ilmenite in the IBC-rich layer affects not only its density but also the HPE abundances. Less ilmenite in the IBC-rich layer could mean less IBC sinking during cumulate mantle overturn. In this scenario, less HPE (hosted in KREEP) would be entrained with sinking IBC because these two characteristics of the cumulates are likely directly related to each other [*Zhang et al.*, 2013a; *Hess and Parmentier*, 1995]. When less KREEP is entrained, a less dense IBC-rich layer would be able to gain less thermal buoyancy, which will not favor the generation of a single plume.

The present-day CMB temperatures in our models with ilmenite-dependent rheology (Figure 1c and Table S3b) are above the expected solidus for ilmenite-bearing harzburgite [*Yao and Liang*, 2012]. Although the phase equilibria data are limited and preliminary, it is almost inevitable that the stable IBC-rich layers in the three cases would experience extensive melting at early times and very likely remain partially molten to the present day. This may offer an explanation to the suggested low-viscosity, seismically attenuating layer at the base of lunar mantle [e.g., *Nakamura*, 1977; *Wieczorek et al.*, 2006; *Weber et al.*, 2011; *Efroimsky*, 2012; *Khan et al.*, 2014; *Williams et al.*, 2014; *Matsumoto et al.*, 2015; *Harada et al.*, 2016]. A high-temperature layer with partially molten IBC will require a lower sulfur content in the core to produce a 240 km inner core [*Weber et al.*, 2011] and suppress energy loss upon CMB and hence the lunar dynamo growth [*Zhang et al.*, 2013a]. Among our models, the ones with a lower activation energy show a present-day CMB temperature more consistent with joint inversion results [e.g., *Khan et al.*, 2014]. A stable IBC-rich layer, maybe Fe enriched, on the CMB is also consistent with the inverted density profile of *Matsuyama et al.* [2016].

Our model results suggest that for a factor of 10 reduction in IBC-rich layer viscosity, the formation of a global-scale single upwelling is physically unlikely. Thus, the spatial concentration of Ti-rich mare basalts on the lunar nearside by degree 1 upwelling of overturned IBC is also unlikely. Mare basalt source materials could be spatially concentrated on the nearside by spherical harmonic degree 1 downwelling of an IBC diapir [*Parmentier et al.*, 2002; *Elkins-Tanton et al.*, 2002]. This type of long-wavelength downwelling requires a low-viscosity IBC material, consistent with the new experimental data. *Parmentier et al.* [2002] argued that the formation of a single downwelling diapir requires a significantly lower viscosity in the IBC relative to underlying mantle. In cases where the IBC viscosity differences from underlying mantle are removed, a downwelling pattern of many small-scale blobs, without any concentration at the nearside may be expected [e.g., *de Vries et al.*, 2010]. Low IBC viscosity suggested by the rock deformation experiments shed light on mechanisms for forming degree 1 downwelling instabilities [*Li et al.*, 2016]. Our present study emphasizes the importance of better constraining the rheology of ilmenite-bearing lunar mantle. A more complete understanding of IBC rheology requires further experimental work exploring the effects of water [e.g., *Hauri et al.*, 2015], Fe-Mg exchange among IBC constituent minerals [e.g., *Thacker et al.*, 2009; *Dygert et al.*, 2014; *Tokle et al.*, 2017], and strain partitioning between strong and weak phases in multiphase aggregates.

Acknowledgments
This work was supported in part by NASA grant SSERVI NNA14AB01A, a Jackson School of Geosciences Postdoctoral Fellowship to N.D., and funding from Peking University to N.Z. Computational work was supported by Center for Computation and Visualization at Brown University and the Pawsey Supercomputing Centre with funding from the Australian Government and the Government of Western Australia. The input files for reproducing the numerical models can be accessed at nan_zhang@pku.edu.cn. This paper benefited from thoughtful reviews by Andrew Dombard, Walter Kiefer and an anonymous reviewer.

References

Albarede, F., E. Albalat, and C.-T. Lee (2014), An intrinsic volatility scale relevant to the Earth and Moon and the status of water in the Moon, *Meteorit. Planet. Sci.*, 1–10, doi:10.1111/maps.12331.

Binder, A. B. (1982), Post-Imbrain global lunar tectonism: Evidence for an initially totally molten Moon, *Earth Moon Planet.*, *26*, 117.

Canup, R. M. (2012), Forming a Moon with and Earth-like composition via a giant impact, *Science*, *338*, 1052–1055, doi:10.1126/science.1226073.

Christensen, U. (1984), Convection with pressure- and temperature-dependent non-Newtonian rheology, *Geophys. J. R. Astron. Soc.*, *77*, 343–384.

Ćuk, M., and S. T. Stewart (2012), Making the Moon from a fast-spinning Earth: A Giant impact followed by resonant despinning, *Science*, *338*, 1047–1052, doi:10.1126/science.1225542.

de Vries, J., A. van den Berg, and W. van Westrenen (2010), Formation and evolution of a lunar core from ilmenite-rich magma ocean cumulates, *Earth Planet. Sci. Lett.*, *292*, 139–147, doi:10.1016/j.epsl.2010.01.029.

Dygert, N., Y. Liang, C. Sun, and P. Hess (2014), An experimental study of trace element partitioning between augite and Fe-rich basalts, *Geochim. Cosmochim. Acta*, *132*, 17–186.

Dygert, N. (2015), Experimental and field constraints on the physicochemical evolution of the lunar and terrestrial mantles, PhD thesis, Brown Univ.

Dygert, N., G. Hirth, and Y. Liang (2016), A flow law for ilmenite in dislocation creep: Implications for lunar cumulate mantle overturn, *Geophys. Res. Lett.*, *43*, 532–540, doi:10.1002/2015GL066546.
Efroimsky, M. (2012), Tidal Dissipation Compared to Seismic Dissipation: In Small Bodies, Earths, and Super-Earths, *Astrophys. J.*, *746*, 150, doi:10.1088/0004-637X/746/2/150.
Elkins-Tanton, L. T., J. A. Van Orman, B. H. Hager, and T. L. Grove (2002), Re-examination of the lunar magma ocean cumulate overturn hypothesis: Melting or mixing is required, *Earth Planet. Sci. Lett.*, *196*, 239–249, doi:10.1016/S0012-821X(01)00613-6.
Elkins-Tanton, L. T., S. Burgess, and Q.-Z. Yin (2011), The lunar magma ocean: Reconciling the solidification process with lunar petrology and geochronology, *Earth Planet. Sci. Lett.*, *304*, 326–336.
Harada, Y., S. Goossens, K. Matsumoto, J. Yan, J. Ping, H. Noda, and J. Haruyama (2016), The deep lunar interior with a low-viscosity zone: Revised constraints from recent geodetic parameters on the tidal response of the Moon, *Icarus*, *276*, 96–101.
Hauri, E. H., A. E. Saal, M. J. Rutherford, and J. A. Van Orman (2015), Water in the Moon's interior: Truth and consequences, *Earth Planet. Sci. Lett.*, *409*, 252–264, doi:10.1016/j.epsl.2014.10.053.
Hess, P. C., and E. M. Parmentier (1995), A model for the thermal and chemical evolution of the Moon's interior: Implications for the onset of mare volcanism, *Earth Planet. Sci. Lett.*, *134*(3–4), 501–514, doi:10.1016/0012-821X(95)00138-3.
Hirth, G., and D. L. Kohlstedt (2003), Rheology of the upper mantle and the mantle wedge: A view from the experimentalists. Inside the subduction factory, *Geophys. Monogr.*, *138*, 83–105.
Jones, J. H., and H. Palme (2000), Geochemical constraints on the origin of the Earth and Moon, in *Origin of the Earth and Moon*, edited by R. Canup and K. Righter, pp. 197–216, Univ. of Ariz. Press, Tucson.
Jordan, P. G. (1987), The deformational behavior of bimineralic limestone-halite aggregates, *Tectonophysics*, *135*, 185–197.
Karato, S., and P. Wu (1993), Rheology of the upper mantle: A synthesis, *Science*, *260*, 771–778.
Khan, A., J. A. D. Connolly, A. Pommier, and J. Noir (2014), Geophysical evidence for melt in the deep lunar interior and implications for lunar evolution, *J. Geophys. Res. Planets*, *119*, 2197–2221, doi:10.1002/2014JE004661.
Lawrence, K., L. Tauxe, C. L. Johnson, and J. Gee (2008), Lunar paleointensity measurements: Implications for lunar magnetic evolution, *Phys. Earth Planet. Inter.*, *168*, 71–87.
Lin, Y., E. Tronche, E. Steenstra, and W. van Westrenen (2017), Evidence for an early wet Moon from experimental crystallization of the lunar magma ocean, *Nat. Geosci.*, doi:10.1038/NGEO2845.
Li, H., N. Zhang, J. Huang, and N. Dygert (2016), Revisit the lunar overturn model with the ilmenite rheology experiment results, AGU Fall Meeting, DI33A-08.
Lucey, P. G., D. T. Blewett, and B. R. Hawke (1998), Mapping the FeO and TiO_2 content of the lunar surface with multispectral imagery, *J. Geophys. Res.*, *103*(E2), 3679–3699, doi:10.1029/97JE03019.
Matsumoto, K., R. Yamada, F. Kikuchi, S. Kamata, Y. Ishihara, T. Iwata, H. Hanada, and S. Sasaki (2015), Internal structure of the Moon inferred from Apollo seismic data and selenodetic data from GRAIL and LLR, *Geophys. Res. Lett.*, *42*, 7351–7358, doi:10.1002/2015GL065335.
Matsuyama, I., F. Nimmo, J. T. Keane, N. H. Chan, G. J. Taylor, M. A. Wieczorek, W. S. Kiefer, and J. G. Williams (2016), GRAIL, LLR, and LOLA constraints on the interior structure of the Moon, *Geophys. Res. Lett.*, *43*, 8365–8375, doi:10.1002/2016GL069952.
Nakamura, Y. (1977), HFT events: Shallow moonquakes?, *Phys. Earth Planet. Inter.*, *14*, 217–223.
Nakamura, Y. (2003), New identification of deep moonquakes in the Apollo lunar seismic data, *Phys. Earth Planet. Inter.*, *139*, 197–205.
Nyquist, L. E., and C.-Y. Shih (1992), The isotopic record of lunar volcanism, *Geochim. Cosmochim. Acta*, *56*, 2213–2234.
Papike, J. J., G. Ryder, and C. K. Shearer (1998), Lunar samples, in *Planetary Materials*, edited by J. J. Papike, pp. 5-1–5-234, Mineral. Soc. of Am., Washington, D. C.
Parmentier, E. M., S. Zhong, and M. T. Zuber (2002), Gravitational differentiation due to initial chemical stratification: Origin of lunar asymmetry by the creep of dense KREEP, *Earth Planet. Sci. Lett.*, *201*, 473–480.
Qin C. and S. Zhong (2014), Oscillatory thermochemical convection as a cause for the episodic Mare Basalt volcanism in the PKT region of the Moon, AGU Fall Meet. 2014, Abstract DI51A-4352.
Reuss, A. (1929), Berechnung der Fliessgrenze von Mischkristallen auf Grund der Plastizitätsbedingung für Einkristalle, *Z. Angew. Math. Mech.*, *9*, 49–58.
Ringwood, A. E., and S. E. Kesson (1976), A dynamic model for mare basalt petrogenesis, *Proc. 7th Lunar. Sci. Conf.*, *2*, 1697–1722.
Scheinberg, A., L. Elkins-Tanton, and S. Zhong (2014), Timescale and morphology of Martian mantle overturn, *J. Geophys. Res. Planets*, *119*, 454–467, doi:10.1002/2013JE004496.
Snyder, G. A., L. A. Taylor, and C. R. Neal (1992), A chemical model for generating the sources of mare basalts: Combined equilibrium and fractional crystallization of the lunar magmasphere, *Geochim. Cosmochim. Acta*, *56*, 3809–3823, doi:10.1016/0016-7037(92)90172-F.
Stegman, D., M. Jellinek, S. A. Zatman, J. R. Baumgardner, and M. A. Richards (2003), An early lunar core dynamo driven by thermochemical mantle convection, *Nature*, *421*, 143–146.
Stevenson, D., and C. F. Yoder (1981), A fluid outer core for the Moon and its implications for lunar dissipation, free librations, and magnetism, Lunar Planet. Sci. XII, 1043–1045.
Tokle, L., G. Hirth, P. Raterron, C. Holyoke, and N. Dygert (2016), The role of ilmenite content on the rheology of olivine aggregates, AGU Fall Meet., MR23A-2673.
Tokle L., Hirth G., Raterron P., N. Dygert, Y. Liang, and C. W. Holyoke (2017), The pressure and Mg# dependence of ilmenite and ilmenite-olivine aggregate rheology: Implications for lunar cumulate mantle overturn, *LPSC*, XLVIII2017.
Tullis, T. E., F. G. Horowitz, and J. Tullis (1991), Flow laws of polyphase aggregates from end-member flow laws, *J. Geophys. Res.*, *96*(B5), 8081–8096, doi:10.1029/90JB02491.
Taylor, R. S. (1982), *Planetary Science: A Lunar Perspective*, pp. 56–74, Lunar Planet. Inst, Houston, Tex.
Thacker, C., Y. Liang, Q. Peng, and P. C. Hess (2009), The stability and major element partitioning of ilmenite and armalcolite during lunar cumulate mantle overturn, *Geochim. Cosmochim. Acta*, *73*, 820–836, doi:10.1016/j.gca.2008.10.038.
Turcotte, D., and G. Schubert (2002), *Geodynamics*, 2nd ed., pp. 244–248, Cambridge Univ. Press, Cambridge, U. K.
Wang, K., and S. Jacobsen (2016), Potassium isotopic evidence for a high-energy giant impact origin of the Moon, *Nature*, *538*, 487–490.
Warren, P. H. (1985), The magma ocean concept and lunar evolution, *Annu. Rev. Earth Planet. Sci.*, *13*, 201–240.
Weber, R., P. Y. Lin, E. Garnero, Q. Williams, and P. Lognonne (2011), Seismic detection of the lunar core, *Science*, *331*, 309–312.
Wieczorek, M. A., et al. (2006), The constitution and structure of the lunar interior, *Rev. Mineral. Geochem.*, *60*, 221–364.
Williams, J. G., et al. (2014), Lunar interior properties from the GRAIL mission, *J. Geophys. Res. Planets*, *119*, 1546–1578, doi:10.1002/2013JE004559.
Yao, L., and Y. Liang (2012), An experimental study of the solidus of a hybrid lunar cumulate mantle: Implications for the temperature at the core-mantle boundary of the Moon, *LPSC*, 43rd, #2258.

Zhang, N. (2014), *Encyclopaedia of Lunar Science: Internal Structure/Mantle Motions of the Moon*, edited by B. Cudnik, pp. 1–6, Springer, New York.

Zhang, N., E. M. Parmentier, and Y. Liang (2013a), A 3D numerical study of the thermal evolution of the Moon after cumulate mantle overturn: The importance of rheology and core solidification, *J. Geophys. Res. Planets*, *118*, 1–16, doi:10.1029/jgre.20121.

Zhang, N., E. M. Parmentier, and Y. Liang (2013b), Effects of lunar cumulate mantle overturn and megaregolith on the expansion and contraction history of the Moon, *Geophys. Res. Lett.*, *40*, 5019–5023, doi:10.1002/grl.50988.

Zhong, S., M. Parmentier, and M. Zuber (2000), A dynamic origin for the global asymmetry of lunar mare basalts, *Earth Planet. Sci. Lett.*, *177*, 131–140.

Zhong, S., A. K. McNamara, E. Tan, L. Moresi, and M. Gurnis (2008), A benchmark study on mantle convection in a 3-D spherical shell using CitcomS, *Geochem. Geophys. Geosyst.*, *9*, Q10017, doi:10.1029/2008GC002048.